JOURNAL OF MATERIALS SCIENCE **38** (2003) 1737–1745

Deformation and fracture behavior of notched and unnotched unidirectional C/C-Mg composite with Young's modulus 520 GPa and tensile strength 1 GPa

S. OCHIAI*, H. OKUDA
International Innovation Center, Kyoto University, Sakyo-ku, Kyoto 606-8501, Japan
E-mail: ochiai@mtl.kyoto-u.ac.jp; ochiai@mech.kyoto-u.ac.jp

N. SUZUKI
Advanced Materials Technologies, 232-26 Ashitaka-Onoue, Numazu-city, Shizuoka 410-0001, Japan

M. TANAKA, M. HOJO
Graduate School of Engineering, Kyoto University, Sakyo-ku, Kyoto 606-8501, Japan

E. TSUSHIMA
FJ Composites, 701-1 Miyajima, Fiji-city, Shizuoka 416-0945, Japan

Experimental study on tensile fracture behavior of the newly developed C/C-Mg composite, prepared by infiltration of Mg into the pores in the C/C composite heat-treated at 3000°C, was carried out. The volume fraction of the filled Mg was 9–10%. The composite had a specific density 2.1, Young's modulus 520 GPa and Poisson's ratio 0.26. The average tensile strength measured for the specimen with a nominal width 8 mm, gage length 40 mm and thickness 1 mm was 1 GPa. The Young's modulus was improved from 450 to 520 GPa and the strength from 0.9 to 1.0 GPa by Mg-infiltration. The specific Young's modulus and specific strength based on the average measured values were 2.5×10^7 m and 5×10^4 m, respectively, showing high potential as light-weight, stiff and strong structural material. The strength distribution of the composite was described by the two-parameter Weibull distribution function with a shape parameter 7.6 and scale parameter 1060 MPa. Prior to the overall fracture of the composite, the longitudinal cracking arose at the notch tip, due to which the notch tip was blunted and the ligament portion behaved like an unnotched specimen. As a result, the notched strength could be described by the net stress criterion. The apparent critical energy release rate at formation of the longitudinal crack was around 70–90 J/m^2.

1. Introduction

As carbon fiber-reinforced metal matrix composites have high specific strength and high thermal conductivity, they are promising as lightweight structural materials with functionality such as high thermal conductivity and low electrical resistance. In general, they are fabricated by consolidation of fiber and matrix by casting or powder metallurgical method. In this work, as another route, C/C-Mg composite was fabricated by combining the recently developed unidirectional C/C composite [1–3] with magnesium to achieve high mechanical and functional properties. The features of the base C/C composite and the reasons why we used such a base composite to fabricate the C/C-Mg composite are summarized below.

(1) The recently developed unidirectional C/C composite with an average fiber volume fraction 0.59 has the following features. (a) The C/C composite is prepared from prepreg sheets consisting of pitch-based carbon fiber and matrix precursor containing pitch-powder. It is emphasized that the matrix is the mixture of the precursor (phenolic resin) and pitch powder, which makes it possible to produce composite without repeating impregnation and pyrolysis, and to reduce the time for fabrication [1–3]. (b) When the C/C composite is fabricated or heat-treated above 3000°C, the thermal conductivity in the fiber direction becomes very high (450 W/m·K) which is higher than the pure copper (390 W/m·K). The Young's modulus measured by bending test and tensile strength of such composites

*Author to whom all correspondence should be addressed.

are reported to be 450GPa and 900 MPa, respectively [1–4].

(2) The deduction of the theoretical density of the carbon matrix made by carbonization of resin in the C/C composite is difficult, since the matrix involves a large spectrum of structural carbon variants ranging from well-order graphite to vitreous carbon [5]. It is speculated that the matrix of the present base C/C composite is mostly graphite due to the pyrolysis of the mixture of the phenolic resin and pitch powder and high temperature heat-treatment (3000°C), but the detailed amount and distribution of the carbon variants, if exists, within the matrix is unknown. Due to such reasons, the theoretical density could not be estimated accurately. Instead, the upper bound of the theoretical density of the base C/C was deduced approximately as follows, for reference. The highly graphitized fiber has a specific density 2.17 [5]. If we assume that the structure of the matrix becomes to be same as that of fiber due to very high temperature heat-treatment (3000°C), the theoretical density of the C/C composite is deduced to be 2.17. As the measured specific density of the C/C composite is 1.93–1.95 [1, 3, 4], the fraction of pores is calculated to be around 10–11% as an upper bound.

If the vitreous carbon is included in the matrix, the calculated volume fraction of pores in the composite becomes lower, since the specific density of vitreous carbon is low as 1.4 [6]. For instance, if 10% of the matrix is assumed to be vitreous, and 90% of the structure of the matrix to be same as that of fiber, the theoretical density of the base C/C composite with fiber- and matrix volume fractions 0.59 and 0.41, respectively, is calculated to be 2.14. In this case, the volume fraction of the pores of the base C/C composite is calculated to be 9–10%.

As shown above, the pores with around 10% in volume fraction are pre-existent in the base C/C composite, to a first approximation. The formation of the pores stems from the carbonization process of the matrix [1]. In this process, the generated gas goes out through the specimen and the pores are connected like a corridor (open pores). This indicates that there exist paths for the molten metal to be penetrated and thus the pores in the base C/C composite can be replaced by metal. Such a feature could be utilized for fabrication of C/C-metal composite by applying the squeeze casting method. (For the isolated pores (closed pores), the Mg cannot be infiltrated. However, the amount of the closed pores is very small in comparison with that of open pores, as will be shown later in 3.1.)

In the present work, Mg was used as the metal since the weight of C/C-Mg composite will be lighter than that of other metal-included composite such as C/C-Al. The new C/C-Mg composite is expected to have light-weight, high specific strength and high thermal conductivity. In the present work, as a first step, the Young's modulus and tensile strength along the fiber axis of notched and unnotched specimens of this new composite were evaluated and the strength-determining mechanism was discussed.

2. Experimental procedure

The C/C-Mg composite specimens were prepared at Advanced Materials Technology Inc. by a squeeze casting method in which pure Mg was infiltrated into the pores in the base C/C composite with an average fiber volume fraction 0.59 (FC-1030, Advanced Materials International company). The magnesium was molten at 993 K and infiltrated into the base C/C composite preheated to 523 K under a pressure of 100 MPa. By this method, almost all pores of the base C/C composite were filled with Mg, as will be shown later in 3.1.

The plate specimens, with a nominal dimension of width $W = 8$ mm, length $L = 95$ mm and thickness $T = 1$ mm, were used for density measurements and tensile tests. The density of the composite was estimated from the measured volume and weight of the 20 specimens and the result was averaged. In the tensile tests, the longitudinal direction was taken to be parallel to the fiber axis for both notched and unnotched specimens. In the case of unnotched specimens to measure Young's modulus and tensile strength, the gage length was set to be 40 mm, as shown in Fig. 1a. In order to avoid the damage of the specimens in the grips, GFRP (glass fiber-reinforced plastics) tabs were pasted on both ends of the specimens. The strain was measured by the strain gages (Kyowa Dengyo, Ltd., KFG-2-120-C1-11 L1M2R) pasted on the front and back surfaces.

For measurement of the notched strength, the double-edge-notched specimens (Fig. 1b) were used. The relative notch length ($2a/W$ where $2a$ is the notch length) was varied from zero to 0.6 in step of 0.2. The radius of the notch tip was made to be 50 μm with a saw. When the material is notch-sensitive, the behavior and the resultant notched strength are dependent on specimen size. However, it is not the present case; the present composite was not notch-sensitive so that the feature of the fracture of the present composite could be

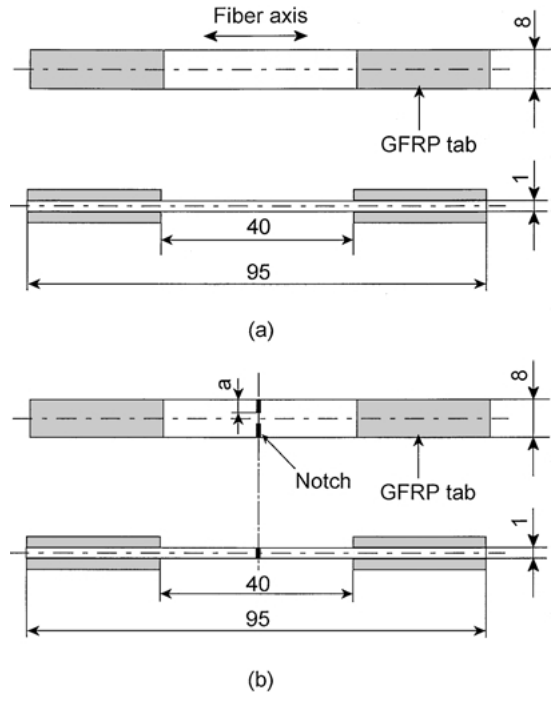

Figure 1 Configuration of (a) unnotched and (b) notched specimens for tensile test.

characterized even though the specimen size was small, as will be shown in 3.4.

The strain gages same as those for unnotched specimens were pasted in the center of the ligament portion between the notches, as shown in Fig. 2a, in order to monitor the preceding longitudinal cracking arising at the notch tip prior to the overall fracture (Fig. 2b). As the length and width of the grid portion in the employed gage were 2 and 1.3 mm, respectively, the gages could be pasted within the ligament portion. Once the longitudinal cracking arises, the notch tip is blunted and the stress concentration ahead of the notch tip is reduced [7–9]. Thus the deformation of the ligament in the strain-gage-pasted region comes to be unconstricted to some extent by the notch. With further growth of the longitudinal crack (Fig. 2c), the constriction of the deformation of the ligament decreases more. When the front of the longitudinal crack goes far away from the gage-pasted region, the gage-pasted region deforms as if there were no notch. Under such a situation, only the ligament portion supports the applied stress. Thus, the slope in the stress-strain relation of the strain gage-pasted portion, being proportional to the inverse compliance, is high in the early stage up to the onset of the longitudinal crack, but then it decreases with growth of longitudinal crack and approaches to $(1 - 2a/W)E_c$ where E_c is the Young's modulus of the composite. Thus the stress of composite σ_c will vary as schematically shown in Fig. 2d with increasing strain ε measured by the pasted strain gages. In this way, the obtained $\sigma_c - \varepsilon$ curve can be used to monitor the growth of the longitudinal crack.

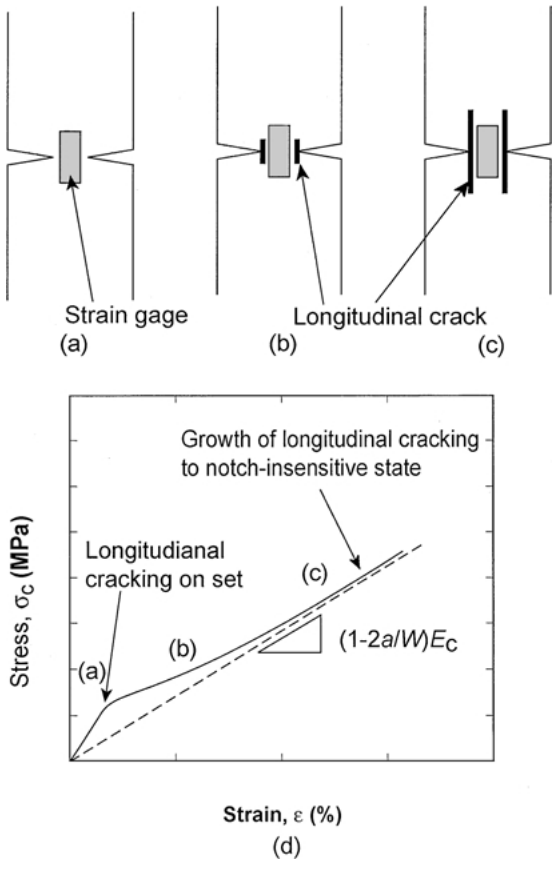

Figure 2 Schematic representation of the geometrical relation of the pasted strain gage to the longitudinal crack, and the feature of the stress-strain curve of the notched specimens. When the longitudinal crack, in the notched specimen with the pasted strain gage as in (a), grows as in (b) and (c), the resultant stress-strain curve varies as shown in (d).

Tensile test was carried out at room temperature at a crosshead speed of 8.3×10^{-3} m/s using the autograph (AG-50kNG, Shimadzu Co. Ltd.). Test control, and also the recording and analysis of the data, were carried out with a computer-aided system (SHiKiBU, Shimadzu Co. Ltd.). The fracture surface was observed at an accelerating voltage of 15 kV with a scanning electron microscope (JSM-5410LS, Joel Co. Ltd). The distribution of the infiltrated Mg was examined by an electron probe microanalyzer (X-650, Hitachi Co. Ltd.)

3. Results and discussion

3.1. Microstructure and density of the fabricated C/C-Mg composite

Fig. 3 shows (a, b) the appearance of the polished transverse cross-section in the central region of the fabricated C/C-Mg composite and (c) the distribution of the Mg element in (b). The result of observation of the microstructure shows the followings. (i) From the comparison of Fig. 3b with c, the white portions in (a) and (b) were identified to be the Mg-filled pores. It is noted that Mg filled not only into the pores near the surface region but also in the central region far from the surface of the composite (Fig. 3a and b). (ii) As the pores exist both at interface and in matrix, Mg went to both. The Mg at the interface was expected to improve the stress transfer efficiency through the diminishment of the interface-pores and to reduce the stress concentration arising from the fiber-breakage through the plastic deformation. In addition, the Mg in the matrix was expected not only to reduce the amount of preexistent pores but also to suppress the matrix-breakage. Accordingly, the improvement of stress carrying capacity of the carbon matrix was also expected.

As shown above, the microstructure observation revealed that the pores were filled with Mg. Such a feature of the present C/C-Mg composite was reconfirmed from the density measurements as follows. The specific density of the fabricated C/C-Mg composite, measured for 20 specimens, was 2.10 on an average. As the specific densities of the base C/C composite and Mg are 1.93–1.95 [1, 3, 4] and 1.74, respectively, the volume fraction of the filled Mg was estimated to be around 9–10%. This result also demonstrates that almost all pores were filled with Mg, since the volume fraction of the pores of the base C/C composite was around 10% (or less if the whole matrix was not fully graphitized, as shown in Introduction.)

The Mg cannot go into the closed pores. Therefore, if the amount of the closed pores is large, high efficiency of Mg-infiltration cannot be achieved. However, it is not the present case, since the pores are filled with Mg as shown in Fig. 3 and the volume fraction of the filled-Mg is nearly the same as that of the pre-existent pores, as mentioned above. Summarizing these results, the amount of the closed pores of the base C/C composite was very small, almost all pores were filled with

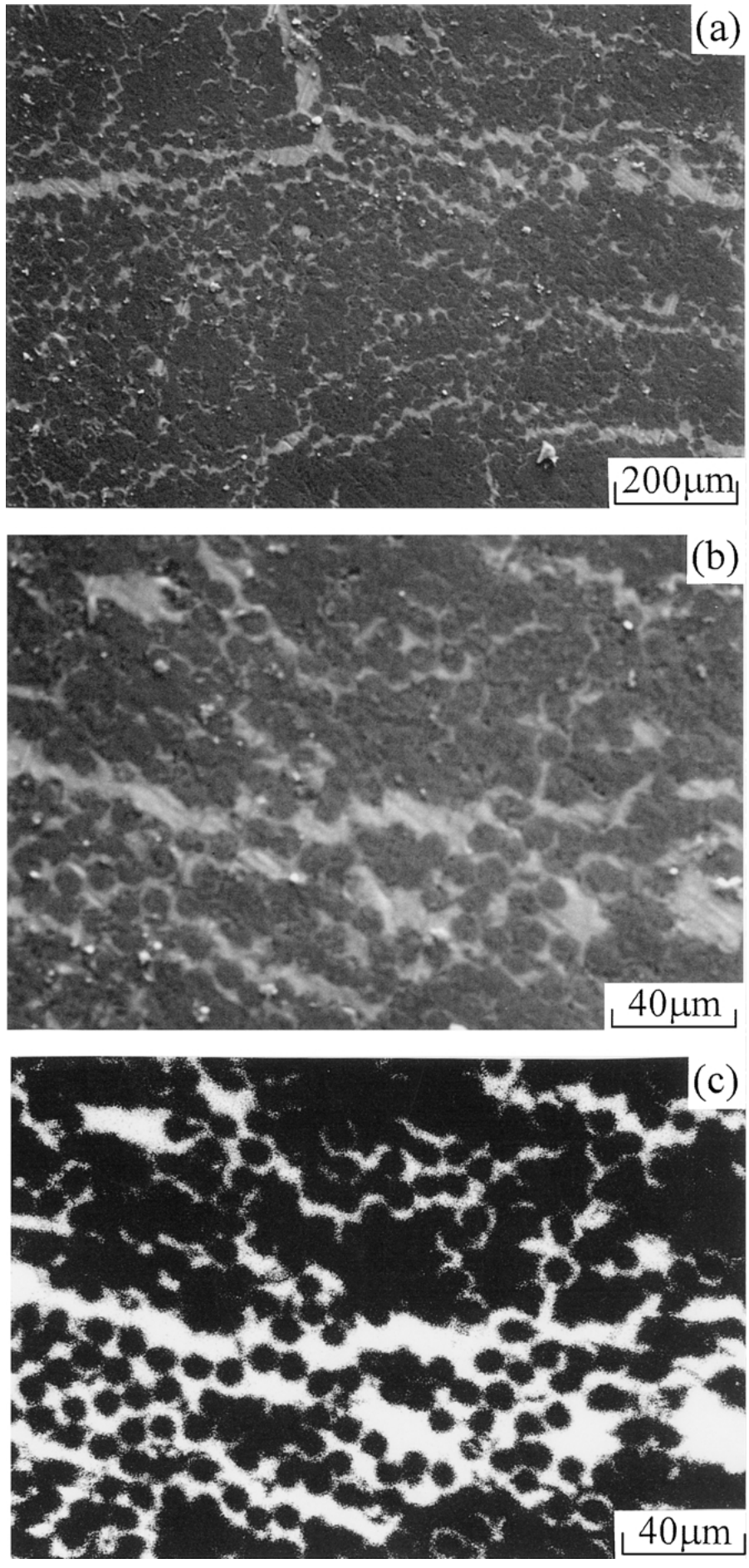

Figure 3 Distribution of Mg in the C/C-Mg composite. (a) and (b): Polished transverse cross-section in the center of the fabricated C/C-Mg composite. The white portions correspond to Mg. (c): Distribution of Mg-element in (b) measured with an electron probe micro analyzer. The white dots correspond to Mg.

Mg and very effective Mg-infiltration was achieved in the C/C-Mg composite.

3.2. Young's modulus E_c and Poisson's ratio ν_c of unnotched specimens

Fig. 4 shows the measured curves of stress σ_c-longitudinal strain ε and σ_c–lateral strain ε_T. While the measured values of ε_T are minus, they are shown in absolute values for convenience in this figure. The linear relation between σ_c and ε and that between σ_c and ε_T were kept apparently in almost whole range of the applied strain and they deviate in the late stage near the overall fracture. The Young's modulus E_c and Possion's ratio ν_c of the composite were estimated from the ratios of σ_c/ε and $\varepsilon_T/\varepsilon$ in the linear range, respectively. The result is listed in Table I.

In the present specimens, the coefficient of thermal expansion of Mg ($\alpha_{Mg} \approx 25 \times 10^{-6}$/K [10]) is higher than that of the base C/C-composite ($\alpha_{C/C} \approx 0$ and 10×10^{-6}/K for longitudinal and transverse directions, respectively [2].) The strain mismatch due to the difference in thermal expansion is $(\alpha_{C/C} - \alpha_{Mg})\Delta T \approx 1.1\%$ if $\alpha_{C/C}$ is taken to be 10×10^{-6}/K, where ΔT is the temperature difference between fabrication- and room temperature (≈700 K). The yield stress of cast pure Mg has been reported to be 21 MPa [11] and that of annealed sheet Mg to be 69 MPa [12]. As the Young's modulus of Mg is around 40 GPa, the yield strains are 0.005 and 0.018% for the former and latter yield stress-values. The mismatch strain (1.1%) is far higher than the yield strain of Mg, from which Mg is inferred to be yielded. Thus the present measured values of E_c and ν_c may not be real elastic constants due to the yielding of the Mg. However, they are, to a first approximation, similar to the values for the elastic state since the contribution of Mg to overall Young's modulus E_c and Poisson's ratio ν_c is small, as shown below.

The volume fraction of Mg is around 9–10% and the Young's modulus is 40 GPa. Thus the contribution of Mg to the Young's modulus of the composite E_c (520 GPa) is around 4 GPa, which is around 0.8% of E_c. Thus the difference in E_c between elastic and plastic states of Mg is in the experimental error. Also, from the rule of the mixtures, the contributions of Poisson's ratio of Mg in elastic (0.3) and plastic (0.5) states to overall Poisson's ratio of the composite are around 0.03 and 0.05, respectively, for 9–10% Mg volume fraction. The difference in ν_c between the elastic and plastic states of Mg is 0.02, which is around 8% of the average measured value of 0.26. In this way, even though Mg is inferred to be yielded, the obtained values of E_c and ν_c in the present work are nearly the same as those for elastic state.

TABLE I Measured tensile strength, Young's modulus and Poisson's ratio

Specimen no.	Tensile strength (MPa)	Young's modulus (GPa)	Poisson's ratio
1	1120	502	0.247
2	950	551	–
3	1110	501	0.246
4	1020	533	0.225
5	914	496	0.264
6	940	468	0.259
7	816	506	0.240
8	1030	501	0.278
9	902	516	–
10	965	510	–
11	1170	547	–
12	1150	516	–
13	777	577	0.278
14	881	542	–
15	1230	562	0.261
Average	998	522	0.255

It is emphasized that the Young's modulus of the base C/C composite (450 GPa) was improved to 520 GPa by Mg-infiltration. Such a big improvement cannot be accounted for by the direct contribution of Mg, since the direct contribution of Mg is at most 4 GPa as stated above. Following indirect contributions of the filled Mg can be mentioned for the improvement.

(A) Improvement of the continuity of the matrix. The matrix of the base C/C composites has many pores.

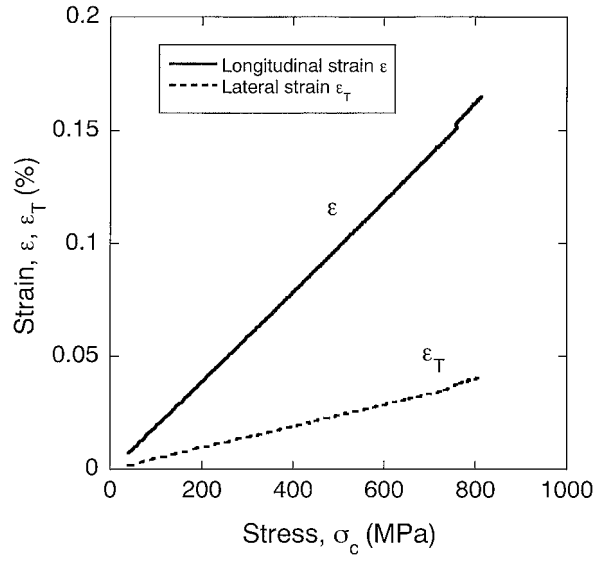

Figure 4 Measured relation of composite stress σ_c to longitudinal strain ε and lateral strain ε_T.

Thus some parts of the matrix are not necessarily connected to each other; namely there exist discontinuous portions, which cannot carry applied stress. By Mg-infiltration, such a discontinuity diminishes. As a result, such portions become to carry applied stress, contributing to the composite Young's modulus. Such a case has been shown by a computer-aided Monte Carlo-shear lag simulation for SiC/TiAl composite [13]; when the matrix is discontinuous, the average axial strain of matrix is low, resulting in low composite Young's modulus due to the insufficient contribution of the matrix, but when the matrix is continuous, the strain of matrix becomes the same as that of fiber, resulting in high composite Young's modulus.

(B) Improvement of the stress transfer-efficiency. The infiltrated Mg at the interface acts to transfer more stress to the fibers through the interface. In addition, the Mg-infiltrated matrix can deform more also in shear without cracking, raising the stress transfer efficiency, too. Thus, the applied stress can be transferred more efficiently, resulting in the higher Young's modulus of the composite.

It is emphasized here that the Young's modulus and specific Young's modulus are very high (520 GPa and 2.5×10^7 m, respectively). Within the knowledge of the authors, these values are highest reported so far for metal-included composites.

3.3. Fracture behavior and strength of unnotched specimens

3.3.1. Fracture behavior

Figs 5 and 6 show the fracture surface of the unnotched specimens. Following features were observed.

1. The composite is broken like a bamboo as shown in Fig. 5a. The composite is divided into several strips and the location of the fracture surface of each strip is different. As shown later in 3.4, this composite has the feature that longitudinal cracking occurs at the notch tip in the case of notched specimen, which suppresses the transverse propagation of the notch. As a result, the strength of the notched specimens becomes notch-insensitive. This suggest that, even if a crack is formed by the fracture of weak portion in the unnotched specimens, the propagation of the crack into transverse direction is suppressed due to the occurrence of the longitudinal cracking at the boundary between the cracked and the neighboring portions. Thus the damages caused by fracture of weaker portions do not grow in transverse direction and therefore they can be accumulated. As a result, the composite is divided into several strips accompanying the longitudinal cracking. Under such a situation, the strips are broken at their weak portions. Thus the location of the fracture surface of each strip was different to each other as in bamboo.

2. As shown in Fig. 5b and c, the fibers were pulled-out, indicating the interface is not strong enough to suppress interfacial debonding.

3. In the fracture surface caused by the longitudinal cracking (Fig. 6), mostly interfacial debonding was found, but partly magnesium adhering to the side surface of the fibers was also found. The macroscopic longitudinal crack cannot arise unless the fracture of matrix between the fibers occurs in addition to the interfacial debonding. On this point, the filled Mg in the matrix is expected to act to resist the longitudinal cracking, causing stable propagation of the longitudinal crack due to its ductility. Such a stable longitudinal crack growth in the present composite will be demonstrated later in Fig. 9 in which the composite stress varies gradually with growing longitudinal crack. Such a gradual variation of the composite stress does not arise when the longitudinal crack grow unstably which causes sudden drop of composite stress [14].

3.3.2. Unnotched strength

The measured strength-values of unnotched specimens with a configuration shown in Fig. 1 are listed in Table I. The average value was 1 GPa, which was higher than the strength of magnesium alloys (360 MPa for ZC71-T6 alloy [12]) and 460 MPa for the particle/intermetallics–reinforced magnesium composite [15, 16]). The reason, why the present fiber-composite had high strength,

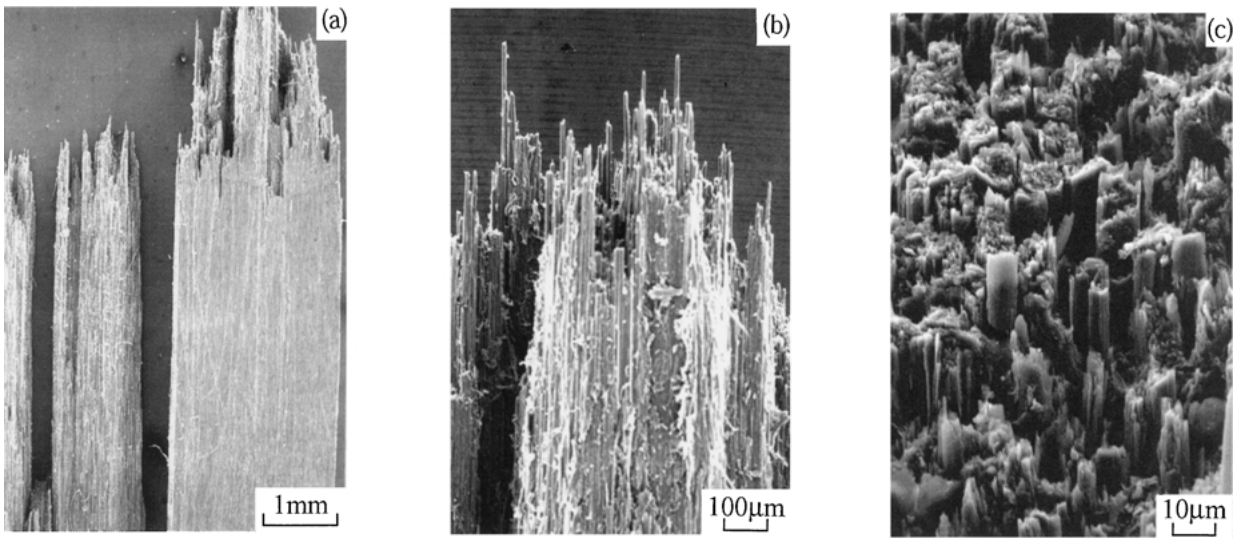

Figure 5 Fracture surface of unnotched specimens.

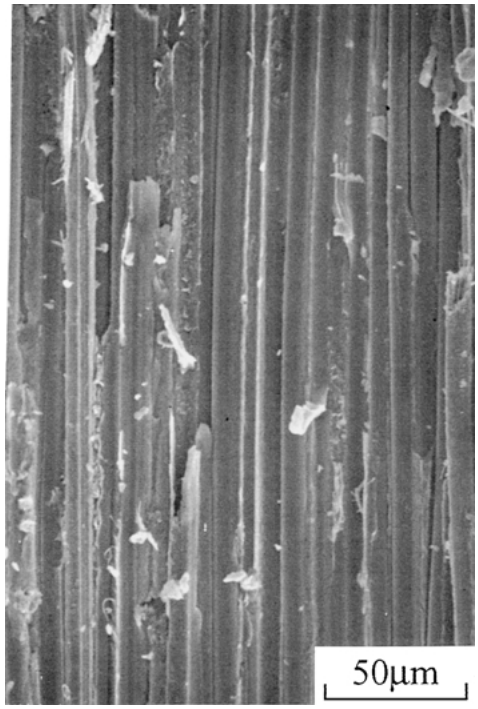

Figure 6 Fracture surface caused by longitudinal cracking in unnotched specimens.

could be attributed to the same mechanism as bamboo as shown above in (A); the crack propagation in transverse direction is suppressed by the premature longitudinal cracking. It is noted that the average strength (1 GPa) is improved by 100 MPa from that of the base C/C composite [1–3], which could be attributed to the suppression of transverse crack propagation and to the higher efficiency of stress transfer due to the infiltrated Mg as stated in 3.2 for improvement of Young's modulus. It is emphasized here that the specific strength is 5×10^4 m. Such a high specific strength, together with the high specific Young's modulus (2.5×10^7 m as shown in 3.2), indicates the high potential of this composite as light-weight, stiff and strong structural material.

The strength distribution of materials can, in most cases, be described by the Weibull distribution function [17]. Whether the unnotched strength σ_{cU} of the present composite obeys the Weibull distribution function or not, was examined as follows. The cumulative function of this distribution, F, is expressed by

$$F = 1 - \exp\{-(L/L_0)(\sigma_{cU}/\sigma_0)^m\} \quad (1)$$

where L is the gage length, L_0 the standard length, σ_0 the scale parameter and m the shape parameter. When the $\ln\ln(1 - F) - 1$ is plotted against $\ln(\sigma_{cU})$ (Weibull plot), the values of m and σ_0 can be estimated from the slope and the extrapolation, respectively, if the linearity between $\ln\ln(1 - F) - 1$ and $\ln(\sigma_{cU})$ is good. The result of the Weibull plot of the strength of the present composite is shown in Fig. 7. The coefficient of determination of the linearity was 0.98, indicating that the strength of the present composite obeys the Weibull distribution function. As a result, the values of m and σ_0 for $L_0 = 40$ mm (gage length) were estimated to be 7.6 and 1060 MPa, respectively.

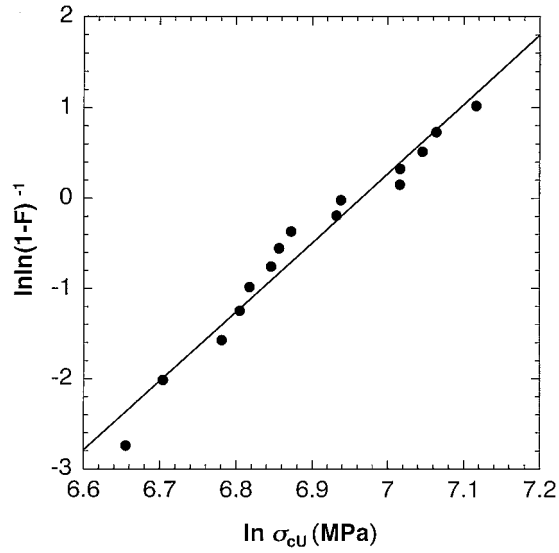

Figure 7 Weibull plot of the measured tensile strength of unnotched specimens.

3.4. Fracture behavior and strength of notched specimens

3.4.1. Fracture behavior

In practical engineering application, the fracture occurs mostly at the stress concentration sources such as notches and defects. In this part, the fracture behavior and strength of notched specimens are studied.

As has been shown above, the longitudinal cracks have been observed in unnotched specimens. In the case of notched specimens, the longitudinal cracking also occurred at the notch tip (Fig. 8), and consequently the notch did not propagate into the transverse direction due to the premature growth of the longitudinal crack.

Fig. 9 shows the relation of the overall composite stress σ_c to the strain ε measured by the strain gage pasted on the specimen (Fig. 2). For comparison, the

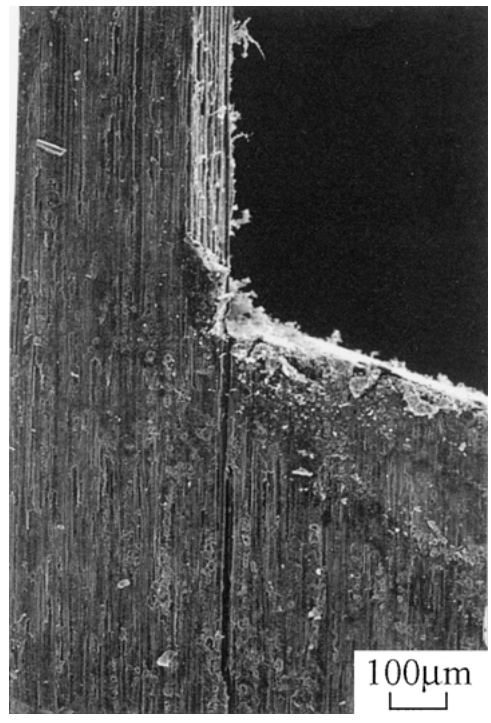

Figure 8 Longitudinal crack at the notch tip.

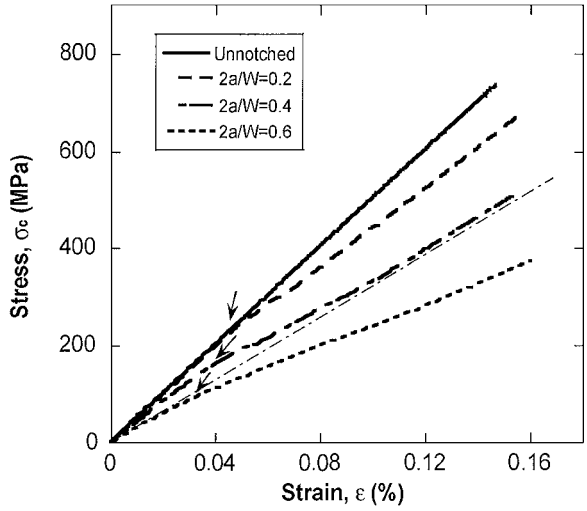

Figure 9 Measured relation of stress of composite σ_c to the strain ε measured by the strain gages pasted on the notched specimens.

stress-strain relation for the assumed case where the longitudinal crack exists over the entire length is drawn with a thin chain line for $2a/W = 0.4$. The measured stress-strain curve (the thick chain curve) approaches gradually to the thin chain line in the high strain range. Such a gradual variation of the composite stress with growing longitudinal crack shows that the crack grows stably, since the sudden drop of composite stress occurs in the stress-strain curve in the case of unstable growth [12].

The constriction caused by the notch is released due to the gradual growth of the longitudinal crack in the present composite, as shown above. The arrows show the deviation points from the linear relation between stress (σ_c) and overall strain (ε), corresponding to the occurrence of the longitudinal cracking. The stresses of the composite at the deviation points, measured from the stress-strain curves in Fig. 9, are listed in Table II. The larger the relative notch length ($2a/W$), the lower becomes the composite stress at formation of the longitudinal crack, as predicted by the model calculation [18, 19].

The longitudinal crack occurred accompanied by the interfacial debonding and matrix fracture (Fig. 6). Which of them controls the formation of the longitudinal cracking behavior was not identified within the present work. Instead, the apparent critical energy release rate at formation of the macroscopic longitudinal crack was estimated based on the method proposed in our work [19]. In this method, the fiber, matrix and interface are not distinguished and the composite is regarded to be composed of strips of mini-composites to a first approximation. Substituting the measured composite stresses at the deviation point from the linear relation between stress and strain into the calculation method, we had the results listed in Table II. The results indicate that the apparent critical energy release rate at formation of the longitudinal crack of the present composite is around 70 to 90 J/m^2.

TABLE II Measured stress of the composite at the deviation from the linear relation between the stress and strain shown with arrows in Fig. 9 and the estimated apparent critical energy release rate at formation of the longitudinal crack

Relative notch length $2a/W$	Stress of composite at deviation (MPa)	Apparent critical energy release rate (J/m^2)
0.2	220–240	72–86
0.4	150–170	79–99
0.6	95–110	62–83
		Ave. 71–90

3.4.2. Notched strength

Fig. 10 shows the measured fracture strength $\sigma_{c,N}$ plotted against $2a/W$. If the composite is assumed to be notch-sensitive, namely if no premature longitudinal cracking occurs and if the damage zone ahead of the notch tip is not large, the fracture mechanical criterion (fracture occurs when the stress intensity factor reaches the critical value) can be applied. Under this criterion, the strength value is proportional to around $a^{-1/2}$. As a result, the strength decreases more sharply with increasing $2a/W$ than that based on the net stress criterion for notch-insensitive materials shown below. Such a fracture mechanical criterion applicable to notch-sensitive materials has been observed for some woven C/C composites which do not show longitudinal cracking [20, 21] and even for ductile matrix composite reinforced with brittle fibers such as Nb_3Al/Cu which also does not show longitudinal cracking [22]. It is, however, not the present case as shown below.

When the premature longitudinal cracking occurs over the entire gage length and there arise no interaction between the separated two portions, the stress singularity at the notch tip is lost; namely the notch tip is blunted. Under this condition, the composite fractures when the stress of the ligament reaches the tensile strength (net stress criterion). Thus, the strength decreases linearly with increasing $2a/W$ as shown with the solid line ($\sigma_{c,N} = \sigma_{cU}(1 - 2a/W)$). It has been demonstrated that such a net stress criterion describes well the notched strength of the weakly bonded C/C [23, 24] and SiC/SiC [25] composites and also of the ductile fiber/ductile matrix composite such as Nb-Ti/Cu [26]. Also intermediate case has been reported for SiC/BMAS

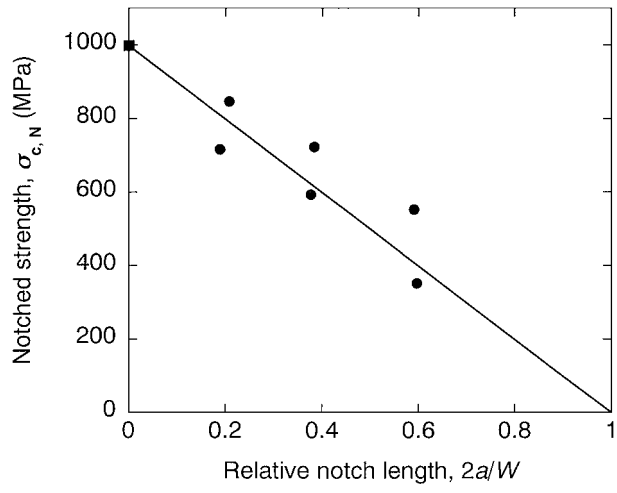

Figure 10 Measured fracture strength $\sigma_{c,N}$ plotted against $2a/W$. The solid line shows the net stress criterion.

(barium magnesium aluminosilicate-glass), whose notched strength is higher than the value predicted by the fracture mechanical criterion due to the blunting arising from the premature longitudinal cracking but it is lower than the value predicted by the net stress criterion due to the constraint effect arising mainly from the bridging of the fibers [19]. The strength of the present composite is described by the net stress criterion, as shown in Fig. 10, indicating that the present composite is notch-insensitive.

4. Conclusions

The mechanical behavior of the newly developed C/C-Mg composite, fabricated by infiltration of Mg into the pores in the base unidirectional C/C composite, was studied. Main results are summarized as follows.

1. The specific density, Young's modulus and specific Young's modulus of the composite were 2.1, 520 GPa and 2×10^7 m, respectively. The Young's modulus was improved from 450 to 520 GPa by Mg-infiltration.
2. The Poisson's ratio is 0.26.
3. The features of tensile fracture of unnotched specimens are summarized as follows.
   (a) The crack arrest mechanism is similar to bamboo on the point that the propagation of the transverse crack to cause overall fracture is suppressed by longitudinal cracking.
   (b) The average tensile strength (measured for the specimen with a nominal width 8 mm, gage length 40 mm and thickness 1 mm) and the specific strength are high; 1 GPa and 2.5×10^4 m, respectively. The strength was improved from 0.9 to 1.0 GPa by Mg-infiltration.
   (c) The strength distribution of the composite strength is described by the two parameter-Weibull distribution function with a shape parameter 7.6 and scale parameter 1060 MPa.
4. The features of fracture of notched specimens are summarized as follows.
   (a) The longitudinal cracking arises at the notch tip.
   (b) As a result of the longitudinal cracking, the notch tip is blunted and the ligament portion behaves like a unnotched specimens
   (c) The notched strength is described by the net stress criterion.
   (d) The apparent critical energy release rate at formation of the longitudinal crack is around 70–90 J/m^2.

Acknowledgements

The authors wish to express their gratitude to Japan Science and Technology Corporation for the support of this work under the original study result-fostering project (No. 0382 in 2000).

References

1. E. TSUSHIMA, J. TAKAYASU, K. TANIGUCHI and A. SHINDO, in Proc. 3rd Symp. on High-Performance Materials for Severe Environment, Sponsored by R & D Institute of Metals and Composites for Future Industries and Japan Industrial Technology Association, Tokyo, 1992, p. 99.
2. J. TAKAYASU, E. TSUSHIMA and T. IZUMI, in Proc. 6th Symp. on High-Performance Materials for Severe Environment, Sponsored by R & D Institute of Metals and Composites for Future Industries and Japan Industrial Technology Association, Tokyo, 1995, p. 293.
3. E. TSUSHIMA and N. KAWAMURA, *Engineering Materials*, **46**(12) (1998) 68.
4. *Idem.*, *ibid.* **47**(3) (1999) 65.
5. R. PLEGER and W. BRAUE, in "Advanced Aerospace Materials," edited by H. Buhl, (Sringer-Verlag, 1992) 203.
6. Nippon Graphite Fiber Co. Ltd.: Technical data sheet of granoc yarn, home page on Web site, Version 2002.08.09.
7. S. OCHIAI, K. OSAMURA, K. TOKINORI, M. NAKATANI and K. YAMATSUTA, *Metall. Trans.* **22A** (1991) 2085.
8. S. OCHIAI and K. OSAMURA, *J. Mater. Sci.* **27** (1992) 4061.
9. S. OCHIAI and M. HOJO, *ibid.* **31** (1996) 3861.
10. O. IZUMI in "Non-Ferrous Materials," edited by Japan Institute of Metals (Maruzen, Tokyo, 1987) p. 119.
11. H. E. BOYER and T. L. GALL (eds.), "Metals Handbook Desk Edition" (ASM, Ohio, 1985) p. 14.7.
12. E. A. BRANDES and G. B. BROOK (eds.), "Smithells Metals Reference Book," 7th ed. (Butterworth-Henemann, 1992) p. 22, 22.
13. S. OCHIAI, T. FUJITA, M. TANAKA, M. HOJO, K. MIYAMURA, H. NAKAYAMA, M. YAMAMOTO and M. FUJIKURA, *J. Japan Inst. Metals* **64**(1) (2000) 7.
14. S. OCHIAI, B. FIEDLER, M. HOJO and K. SCHULTE, *Comp. Interfaces* **7** (2001) 459.
15. S. F. HASSAN and M. GUPTA, *J. Mater. Sci.* **37** (2002) 2467.
16. *Idem. Mater. Res. Bull.* **37** (2002) 377.
17. W. WEIBULL, *J. Appl. Mech.* **18** (1951) 293.
18. S. OCHIAI, M. TANAKA and M. HOJO, *Comp. Interfaces* **5** (1998) 437.
19. S. OCHIAI, I. OKUMURA, M. TANAKA, M. HOJO, M. SATO, M. TAMURA, Y. KOHTOKU and T. YAMAMURA, *J. Mater. Sci.* **35** (2000) 3497.
20. F. E. HEREDIA, S. M. SPEARING, T. J. MCKIN, M. Y. HE and A. G. EVANS, *J. Amer. Cer. Soc.* **77** (1994) 2817.
21. H. HATTA, Y. KOGO, H. ASANO and H. KAWADA, *Trans. Japan Soc. Mech. Eng.*, Ser. A **36** (1998) 897.
22. S. OCHIAI, M. OHNO, T. SAWADA, F. SEKINO, M. HOJO, Y. YAMADA, K. TAKAHASHI, N. AYAI and K. WATANABE, *Sucpercond. Sci. Technol.* **12** (1999) 499.
23. Y. YATOMI, M. HOJO, M. TANAKA, S. OCHIAI, Y. SAWADA and J. TAKAHASI, *J. Soc. Mater. Sci., Japan* **47** (1998) 939.
24. Y. KOGO, H. HATTA, H. KAWATA and T. MACHIDA, *J. Comp. Mater.* **32** (1998) 1273.
25. M. TANAKA, S. OCHIAI, M. HOJO, T. ISHIKAWA, S. KAJII, K. MATSUNAGA and T. YAMAMURA, *Key Eng. Mater.* **104–165** (1999) 141.
26. S. OCHIAI, Y. OKI, F. SEKINO, H. OHNO, M. HOJO, H. MORIAI, S. SAKAI, M. KOGANEYA, K. HAYASHI, Y. YAMADA, N. AYAI and K. WATANABE, *Supercond. Sci. Tech.* **13** (2000) 396.

Received 17 April 2002
and accepted 16 January 2003